Atmos. Chem. Phys. Discuss., 12, 5487–5517, 2012
www.atmos-chem-phys-discuss.net/12/5487/2012/
doi:10.5194/acpd-12-5487-2012

Atmospheric Chemistry and Physics Discussions

Aerosol-precipitation interactions in the southern Appalachian Mountains

G. M. Kelly[1], B. F. Taubman[2], L. B. Perry[1], J. P. Sherman[3], P. T. Soulé[1], and P. J. Sheridan[4]

[1]Department of Geography and Planning, Appalachian State University, Boone, NC 28607, USA
[2]Department of Chemistry, Appalachian State University, Boone, NC 28607, USA
[3]Department of Physics and Astronomy, Appalachian State University, Boone, NC 28607, USA
[4]National Oceanic and Atmospheric Administration, Earth Systems Research Laboratory, Boulder, CO 80305, USA

Received: 8 February 2012 – Accepted: 12 February 2012 – Published: 21 February 2012

Correspondence to: G. M. Kelly (kellygm@email.appstate.edu)

Published by Copernicus Publications on behalf of the European Geosciences Union.

Abstract

There are many uncertainties associated with aerosol-precipitation interactions, particularly in mountain regions where a variety of processes at different spatial scales influence precipitation patterns. Aerosol-precipitation linkages were examined in the southern Appalachian Mountains, guided by the following research questions: (1) how do aerosol properties observed during precipitation events vary by season (e.g., summer vs. winter) and synoptic event type (e.g., frontal vs. non-frontal); and (2) what influence does air mass source region have on aerosol properties? Precipitation events were identified based on regional precipitation data and classified using a synoptic classification scheme developed for this study. Hourly aerosol data were collected at the Appalachian Atmospheric Interdisciplinary Research (AppalAIR) facility at Appalachian State University in Boone, NC (1110 m a.s.l., 36.215°, −81.680°). Backward air trajectories provided information on upstream atmospheric characteristics and source regions. During the warm season (June to September), greater aerosol loading dominated by larger particles was observed, while cool season (November to April) precipitation events exhibited overall lower aerosol loading with an apparent influence from biomass burning particles. Aerosol-induced precipitation enhancement may have been detected in each season, particularly during warm season non-frontal precipitation.

1 Introduction

The interactions of aerosols, clouds, and precipitation are of particular concern in the Southeastern United States (SEUS) where there is a high concentration of atmospheric aerosols of both natural and anthropogenic origin (Weber et al., 2007). In the Southern Appalachian Mountains (SAM), weather patterns are strongly influenced by topography and frontal activity associated with extra-tropical cyclones. While the major focus of this study is to investigate the association of aerosol properties with precipitation

ACPD
12, 5487–5517, 2012

formation in the SAM, it is important to acknowledge that there is a reciprocal relationship between aerosols and climate that remains poorly understood (Power et al., 2006). Atmospheric aerosols influence weather and climate patterns by altering Earth's surface energy balance and impacting the microphysical processes of cloud formation and precipitation development. However, weather and climate patterns influence aerosol loading and ultimately the chemical, optical, and microphysical properties of aerosols on a variety of scales. This study examines the synoptic controls of precipitation patterns and aerosols in the SAM based on a synoptic classification scheme described by Kelly et al. (2012).

Aerosol climatologies have been constructed based on the optical properties of aerosols produced by various sources, including biomass burning, desert dust, biogenic emissions, and anthropogenic sources (Holben et al., 2001; Bollasina et al., 2007). However, the transport of atmospheric particles from source regions to remote areas is an important component of global climate change research and incorporates processes of aerosol loading and synoptic climatology. Aerosol behaviors are affected by meteorological factors on a variety of scales: microscale climatic factors, such as insolation and humidity, can enhance conversion of gases into particles as well as particle growth; atmospheric stability and convection at the mesoscale can often determine the concentration of aerosols in the atmosphere; and at synoptic levels, source region and variable flow patterns dictate the presence and concentration of atmospheric aerosols (Power et al., 2006). A variety of methodologies have been used in evaluating the synoptic controls of atmospheric aerosols, including ground-based sampling schemes (Power et al., 2006) as well as backward air trajectory analyses (Dorling et al., 1992; Swap et al., 1992; Prados et al., 1999; Brankov et al., 1998; Taubman et al., 2006).

Numerous studies have addressed aerosol-induced precipitation enhancement (Rosenfeld et al., 2002; Rudich and Khersonsky, 2002; Givati and Rosenfeld, 2004; Khain et al., 2004; Bell et al., 2008; Lohmann and Hoose, 2009) and precipitation suppression (Rosenfeld, 2000; Borys et al., 2003; Andreae et al., 2004; Rosenfeld and

ACPD
12, 5487–5517, 2012

Givati, 2006). Aerosols strongly impact the precipitation potential of shallow stratiform clouds that occur below (i.e., under) the −10 °C isotherm (Rosenfeld, 1999, 2000). It has been observed that orographic clouds are particularly sensitive to the indirect effects of anthropogenic aerosols, due to their shallow vertical structure and downwind termination (Borys et al., 2003; Givati and Rosenfeld, 2004, 2005; Jirak and Cotton, 2005; Rosenfeld and Givati, 2006).

This study provides results from 16 months of continuous surface-based aerosol measurements in the SEUS and constitutes the first attempt to identify the linkage between aerosols and precipitation in the SAM. This work constitutes a small piece of the research required to better understand aerosol and precipitation patterns in the SAM and to enhance weather forecasts and modeled future climate scenarios. The reciprocal relationship that exists between aerosols and climate dictates that as changes in climate affect aerosol properties, so do changes in aerosol properties affect climate patterns. It is yet to be fully understood how changes in aerosol properties affecting the SAM may influence atmospheric processes across the region and impact weather and climate patterns as a result.

Currently, global climate models (GCMs) are not equipped to sufficiently parameterize aerosols in order to account for the direct and indirect effects of aerosols on weather and climate patterns (Power et al., 2006). Current circulation models forecast increased variability in precipitation patterns in the SEUS, indicating more intense periods of deluge and drought, as a result of anthropogenic-induced warming (Lynn et al., 2007; Karl et al., 2009; Li et al., 2010). However, the physical processes of aerosol-precipitation interactions and the topographic influences on precipitation are not well understood and are difficult to represent in GCMs (Power et al., 2006). Changes in atmospheric circulation patterns may lead to synoptic-scale conditions that enhance aerosol loading in the SAM. The climatological summer (JJA: June-July-August) of 2010 was one of the hottest periods on record for many regions in the SEUS, and it has been predicted that the region may become drier and warmer in the coming decades (Karl et al., 2009; Li et al., 2010).

ACPD
12, 5487–5517, 2012

While this study provides a short-term preliminary assessment of the patterns and properties of aerosols associated with precipitation patterns in the SAM, more research is required to gain a thorough and conclusive understanding of this relationship.

The primary goals of this study were to investigate aerosol-precipitation interactions in the SAM by addressing the following research questions: (1) how do aerosol properties observed during precipitation events vary by season (e.g., summer vs. winter) and synoptic event type (e.g., frontal vs. non-frontal), and (2) What influence does air mass source region have on aerosol properties? A synoptic classification scheme (Kelly et al., 2012) was created to classify precipitation events in the SAM and summarize them by their synoptic influences. Precipitation events were summarized by seasonal and synoptic variations in aerosol properties.

2 Data and methods

2.1 Precipitation data and event identification

The study area was centered on the Appalachian Atmospheric Interdisciplinary Research (AppalAIR) facility (36.213°, −81.691°; 1110 m) on the campus of Appalachian State University (ASU) in Boone, NC (Fig. 1). Daily precipitation totals at monitoring stations within the study area were analyzed during the period 1 June–30 September in 2009 and 2010 (i.e., warm seasons) and 1 November 2009–30 April 2010 (i.e., cool season). Warm season and cool season events were separated due to the spatial and temporal variability in the stability, synoptic patterns associated with precipitation development, and aerosol loading and types characteristic of each season (Konrad, 1997). The shoulder months of May and October were omitted from this study.

Periods of precipitation were identified from the Boone Automated Weather Observing System (AWOS) hourly weather-type data and corroborated with hourly precipitation data from the Boone Environmental and Climate Observing Network (ECONet) station and daily precipitation totals from the Boone cooperative observer (COOP)

ACPD
12, 5487–5517, 2012

station and the Community Collaborative Rain, Hail, and Snow (CoCoRaHS) network stations (Cifelli et al., 2005) in the town of Boone. Precipitation data were obtained and compiled for analysis from 59 monitoring stations in the CoCoRaHS network and from 16 monitoring stations in the COOP network located above 305 m elevation (Fig. 1). Events that qualified for this study produced measurable precipitation (≥0.25 mm) at one or more of the aforementioned monitoring stations. Events were distinguished from one another by a six-hour time period of no precipitation, and the timing of each event was characterized in terms of beginning, maturation, and ending times based on Boone AWOS hourly weather-type data and consistent with the approach used by Perry et al. (2007, 2010) in their investigations of snowfall in the SAM. The beginning of an event was defined as the hour corresponding with the first report of precipitation of any kind, with a minimum of six hours of no precipitation beforehand; the maturation of an event was defined as the hour corresponding with the heaviest precipitation reports; and the ending of an event was defined as the hour corresponding with the last report of precipitation of any kind.

2.2 Synoptic classification

Events were classified using a synoptic classification scheme developed for this study (Kelly et al., 2012) and adapted from Keim (1996). Events taking place between 1 June and 30 September were defined as warm season events, and those taking place between 1 November and 30 April were defined as cool season events. Events were further classified as frontal or non-frontal events based on archived three-hourly National Centers for Environmental Prediction (NCEP) Service Records Retention System (SRRS) Analysis and Forecast Charts (National Climatic Data Center Service Records Retention System Analysis and Forecast Charts, 2010) and NCEP daily weather maps (National Centers for Environmental Prediction Daily Weather Maps, 2010). Frontal and non-frontal precipitation events were differentiated due to the synoptic influences on moisture and aerosols. Frontal events were identified by the presence of a frontal boundary within 300 km of the study area, and were identified as cold, warm, stationary,

ACPD
12, 5487–5517, 2012

or occluded, based on SRRS and NCEP weather charts. In the absence of a clear frontal boundary within 300 km of the study area, events were identified as Gulf Lows when precipitation was associated with a low pressure center in the Gulf of Mexico and as Nor'easters if precipitation was associated with a surface cyclone tracking to the northeast. Nor'easters were sometimes associated with a 500 hPa low pressure center passing nearby the study area. Non-frontal events were defined as precipitation occurring in the absence of frontal activity within 300 km from the study area, and these events included convective and orographic processes of precipitation development.

Events were further classified based on spatial coverage. If <75 % of active stations reported measureable precipitation, the events were classified as scattered, whereas if ≥75 % of active stations reported measureable precipitation, the events were classified as widespread. Additionally, events were analyzed according to upper and lower quartile precipitation values, creating subcategories of events representing heavy and light precipitation, respectively. Daily mean composite plots illustrating sea level pressure and geopotential height at 500 hPa were created for each event class (National Oceanic and Atmospheric Administration Earth System Research Laboratory Daily Mean Composites, 2010). Composite plots were created using the NCEP/National Center for Atmospheric Research (NCAR) reanalysis dataset (Kalnay et al., 1996).

2.3 Meteorological data

Meteorological data were collected from the Beech Mountain monitoring station (36.185°, −81.881°; 1678 m), located approximately 17.4 km west and of AppalAIR (Fig. 1). Average temperature, relative humidity, wind speed, and wind direction values were collected from the State Climate Office of North Carolina Climate Retrieval and Observations Network of the Southeast (CRONOS) and were compiled for beginning and maturation hour of each event and summarized by event type. Average wind direction values were calculated as unit-vector averages, and most frequent wind directions were determined by analysis of a histogram of observed wind directions during each event. In contrast to Boone and other valley or ridge-top locations, wind direction at

ACPD
12, 5487–5517, 2012

Beech Mountain is not considerably controlled by local topography, and data from this location are therefore broadly representative of lower tropospheric (~825 hPa) meteorological conditions. Meteorological data from BEECHTOP were not available from 26 December 2009 through 10 January 2010 due to severe ice and wind causing catastrophic tower collapse.

2.4 Aerosol data

The AppalAIR site has been a NOAA/Earth System Research Laboratory (NOAA/ESRL) Global Monitoring Division (GMD) Collaborative Surface Aerosol Monitoring Network site since 1 June 2009. Because of the height of the tree canopy at the site, aerosol samples are collected from the top of a 34 m above ground level (a.g.l.) sample inlet (~20 cm internal diameter). As a result, the AppalAIR site is typically only 300–500 m below the cloud layer and measurements are arguably representative of the bottom of the moist layer, which is significant in sampling feeder clouds related to orographic precipitation processes. CCN were not directly measured at this site, although that measurement will eventually be possible there. The aerosol sampling protocol used is the same one employed at all NOAA-ESRL collaborative aerosol monitoring sites (Sheridan et al., 2001). The inlet is outfitted with a stainless rain cap and mesh screen to keep birds and insects out. Total flow through the stack is ~1 m^3 min^{-1}. Roughly 150 m^3 min^{-1} is taken from the center of the main stack and directed through a stainless tube (~5 cm internal diameter) to supply the instruments in the facility. This inlet is heated to maintain a RH of ≤50 % prior to entering the facility. Once inside the facility, the inlet is heated a second time to decrease the RH to ≤40 % and divided into five individual sampling lines at 30 l min^{-1}. The remaining flow is either directed to additional instrumentation that will not be discussed in this paper or is exhausted through a blower and filter outside the facility.

Size-segregated aerosol light scattering and absorption is measured with a switched impactor system. A solenoid valve is used to switch the flow every ten minutes between 1-μm aerodynamic diameter cutpoint and 10-μm aerodynamic diameter cutpoint

ACPD
12, 5487–5517, 2012

multiple orifice impactors to achieve 1-µm ($D_p < 1$ µm) and 10-µm ($D_p < 10$ µm) size cuts. Size-segregated aerosol scattering and absorption coefficients (for particles with aerodynamic diameters less than 10 µm and less than 1 µm) were measured using a 3-wavelength (450, 550, and 700 nm) integrating nephelometer (TSI Model 3563) and a 3-wavelength (467, 530, 660 nm) Particle Soot Absorption Photometer (PSAP, Radiance Research, Inc.), respectively. Absorption values were corrected for instrument-specific differences in flow rate, spot size, and also for aerosol scattering and filter matrix influences (Bond et al., 1999). The nephelometer was calibrated with CO_2 and particle-free air and corrections were made to account for angular non-idealities within the nephelometer (Anderson and Ogren, 1998).

All aerosol properties used in this study (Table 1) were for the sub-10 µm particles, as this size limit accounted for the optical properties of virtually all aerosols measured at AppalAIR. Average aerosol properties during the 6 h prior to event beginning were analyzed in order to determine patterns in these values leading up to the onset of precipitation. Aerosol properties were also analyzed during the beginning and maturation times of each event.

2.5 Trajectory analysis

The NOAA Air Resources Laboratory (ARL) HYbrid Single-Particle Lagrangian Integrated Trajectory (HYSPLIT) model (version 4) (Draxler and Rolph, 2011) and 40 km Eta Data Assimilation System (EDAS) 3-hourly archive data were used to create 72-h, three-dimensional kinematic backward air trajectories ending at maturation time of each event at the coordinate location of AppalAIR (36.213°, −81.691°). To account for seasonal surface-atmosphere interactions in the lower troposphere at approximately 800 hPa, warm season trajectories were run with an ending height at 2000 m above sea level (a.s.l.), and cool season trajectories were run at 1500 m a.s.l.

For each synoptic class, a cluster analysis was performed on the backward air trajectories associated with the maturation hour of each precipitation event, an approach based on the clustering methodology used by Taubman et al. (2006). HYSPLIT uses

ACPD
12, 5487–5517, 2012

multiple iterations to create clusters of trajectories by calculating the total spatial variance (TSV) among trajectories. In the first iteration, TSV is zero and each trajectory is considered a stand-alone cluster at this stage (i.e., N trajectories = N clusters) (Draxler, 1999). Two trajectories are paired and the cluster spatial variance (SPVAR) is calculated, which is the sum of the squared distances between the endpoints of the paired clusters. TSV is then calculated, which is the sum of all cluster spatial variances, and pairs of clusters that are combined are those with the lowest increase in TSV. For the second iteration, the number of clusters is N-1 since two trajectories were clustered together in the first iteration, resulting in one less stand-alone cluster. The same calculations and comparisons are performed, resulting in the combination of the two clusters with the lowest increase in TSV. Iterations continue until the very last two clusters are combined. After several iterations during the cluster analysis, TSV increases rapidly, indicating that trajectories being combined within the same cluster are not very similar. At this stage, clustering should stop. In a plot of TSV versus number of clusters, the step just before the large increase in TSV indicates the final number of clusters. While some subjectivity was involved in the choice of final number of clusters, a large change in TSV was required and the choice was not arbitrary.

3 Results and discussion

3.1 Synoptic climatology

The synoptic classification scheme resulted in 183 precipitation events during the study period (Fig. 2) (Kelly et al., 2012). There were 123 events during the two warm seasons in the study period, which included precipitation associated with cold, warm, and stationary fronts, as well as non-frontal mechanisms involving shallow upslope flow and terrain-induced convection. Warm season precipitation events lasted an average of 5 h, ranging in duration from 1 to 29 h, and producing an average of 8.9 mm of precipitation. Overall, these precipitation events were characterized by the presence of

ACPD
12, 5487–5517, 2012

the North American Subtropical High (NASH) to the east (e.g., Li et al., 2010), which favored precipitation in the SEUS by the advection of moisture from the Atlantic Ocean and the Gulf of Mexico and resulted in dominant wind directions from the south and northwest (Table 2). During the warm season, the majority of air masses had a Gulf or Atlantic Ocean coastal connection and therefore higher moisture flux (Fig. 2).

This study examined one cool season, composed of 60 precipitation events, which included frontal precipitation associated with cold, warm, and occluded fronts, as well as Gulf lows and Nor'easters (Kelly et al., 2012). Non-frontal mechanisms, such as northwest upslope flow (e.g., Keighton et al., 2009; Perry et al., 2007) were also responsible for some events. Cool season precipitation events exhibited an overall longer duration than warm season events, lasting an average of 16 h and ranging in duration from 1 to 66 h, and producing an average of 13.4 mm of precipitation. Cool season precipitation events were associated with lower pressures over the study area and to the northeast, with higher pressures to the west, suggesting the advection of air from inland areas and much less moisture originating in the Gulf of Mexico or the Atlantic Ocean. Most air masses associated with cool season precipitation events originated west of the study area (Fig. 2), with dominant wind directions from the northwest and south-southeast (Table 2).

3.2 Aerosol climatology

3.2.1 Seasonal variation

Meteorological variables and aerosol properties at beginning and maturation associated with each cluster reveal distinct differences in source region influences during warm season and cool season precipitation events. Scattering values were much higher during warm season precipitation events (Table 3) consistent with the overall regional increase in secondary organic aerosols during this season (Goldstein et al., 2009). Cool season events were characterized by higher b, α_{scat}, and α_{abs} values, consistent with the presence of locally emitted biomass burning particles (Bergstrom et al.,

ACPD
12, 5487–5517, 2012

2002) from wood-burning stoves, which serve as the primary heating source for 6.2 % of occupied housing units in Watauga County (US Census Bureau, 2010) (Table 3).

Synoptic influences and increased scattering and absorption coefficients during warm season precipitation events resulted in significant differences in aerosol values between warm season and cool season precipitation (Table 3). Higher scattering values are driven by secondary organic aerosols during the warm season (Barr et al., 2003), and the presence of overall larger particles during this time of year at event beginning and maturation is evidenced by significantly smaller b and α_{scat} values. The larger warm season ω_o values indicated the presence of relatively greater scattering, likely the result of increased biogenic emissions in the SEUS (Goldstein, 2009). Smaller warm season α_{abs} values suggest the presence of relatively more soot-like carbonaceous particles during this time of year and less biomass burning particles, while larger α_{abs} values during the cool season were consistent with the presence of biomass burning aerosols (Bergstrom et al., 2002) possibly emitted locally as a result of winter wood burning in the SAM.

There was a small, but statistically significant decrease in both scattering and absorption coefficients from 6 h prior to the beginning of the event (beginning-6 h) to maturation during warm and cool season precipitation events, which was consistent with a raining out effect that removed particles from the air during precipitation (Table 3). A significant increase in α_{abs} from beginning to maturation was displayed in both seasons however, possibly the result of low vapor pressure water soluble organic carbon coalescing with the existing particles as relative humidity increased. It is also possible that the increase in α_{abs} at maturation was a result of the atmospheric aging and mixing of black carbon particles, advected from some distance away, with locally emitted sulfate. This would cause black carbon particles to become coated in sulfate and subsequently more hygroscopic than freshly emitted organics and more effective at scattering light as a result of the collection of more scattering materials and a change in fractal shape.

ACPD
12, 5487–5517, 2012

Light warm season precipitation was associated with significantly cooler and windier conditions than heavy warm season precipitation (Table 4). Heavy warm season precipitation events displayed statistically significant lower α_{scat} and higher α_{abs} values (yet not a large difference) during maturation than light events, suggesting a greater presence of larger, more organic particles during periods of heaviest rainfall (Table 4). Heavy warm season precipitation also exhibited significantly higher α_{abs} values during maturation relative to beginning-6 h, indicating that a higher fraction of organic aerosols (effective CCN) relative to soot particles (ineffective CCN) may have enhanced the precipitation intensity in the SAM. That is, during the warm season when there was a relatively larger fraction of soot, differences in the amount of hygroscopic secondary organic aerosols serving as effective CCN may have intensified precipitation. The fact that optical properties suggested that there was a greater fraction of biomass burning aerosols relative to soot during maturation of cool season precipitation (Table 5) likely decreased the importance of variability in these aerosols to precipitation intensity.

3.2.2 Synoptic variation

In the comparison of synoptic event types in this study, only 12 cool season non-frontal precipitation events were analyzed and therefore did not yield statistically significant results. While influenced by very different air mass source regions during the time period of this study (Fig. 3), statistical analysis revealed no significant differences in the meteorological characteristics or aerosol values associated with warm season frontal and non-frontal precipitation events. There was, however, a significant increase in α_{abs} values from beginning-6 h to maturation during precipitation associated with each synoptic type during the warm season, which was consistently seen throughout this study (Table 6). During warm season frontal precipitation, scattering decreased significantly from beginning-6 h to maturation, evidence of particles being rained out. However, during warm season non-frontal precipitation, absorption decreased significantly from beginning-6 h to maturation (Table 6).

ACPD
12, 5487–5517, 2012

There were no significant differences in precipitation between lower and upper quartile aerosol values during warm season frontal precipitation events (Table 7). This may be a result of a "snowplow" effect, in which the leading edge of a frontal boundary accumulates aerosols while approaching the SAM, leading to similar aerosol loading during both light and heavy frontal precipitation events in the warm season. Precipitation totals associated with upper and lower quartile aerosol values did exhibit significant differences during warm season non-frontal precipitation events (Table 7). During maturation, warm season non-frontal precipitation events exhibited significantly higher precipitation totals associated with higher scattering and α_{abs} values and lower α_{scat}. Aerosol properties at AppalAIR are monitored at an elevation that is very close to the cloud base, indicating that this may be evidence of the presence of secondary organic aerosols, predominant in the SEUS warm season (Goldstein et al., 2009), possibly serving as effective CCN.

Analysis of light and heavy warm season non-frontal precipitation revealed statistically significant lower α_{scat} values during heavy events at beginning-6 h. (Table 8), possibly suggesting the presence of larger organic particles serving as effective CCN during heavy precipitation versus light precipitation. There was no statistically significant change in b at maturation between light and heavy warm season non-frontal precipitation, indicating a questionable difference in particle size between these event types; however, scattering and α_{scat} values were significantly lower during heavy events, accompanied by higher α_{abs} values, all of which may indicate the presence of hygroscopic organic aerosols acting as effective CCN during increased warm season non-frontal precipitation (Table 8).

4 Conclusions

In order to examine aerosol-precipitation linkages in the SAM, precipitation events were identified based on regional precipitation data and classified using a synoptic classification scheme developed for this study. Hourly aerosol data were analyzed for each event

ACPD
12, 5487–5517, 2012

to determine seasonal synoptic differences in aerosol optical properties during precipitation events, and backward air trajectory analysis revealed moisture and aerosol source region information.

Average precipitation per event during the warm season was lower than during the cool season. Warm season precipitation events exhibited a wide range of air mass source regions, possibly related to the opposite phases of El Niño Southern Oscillation (ENSO) affecting each season. A large portion of the low-level moisture associated with warm season precipitation originated in coastal areas. Warm season precipitation events were associated with larger and more scattering aerosols, related to phenological and meteorological cycles. Aerosol optical properties consistent with the presence of hygroscopic secondary organic aerosols acting as effective CCN were associated with warm season precipitation events, particularly during non-frontal mechanisms, possibly leading to aerosol-induced precipitation enhancement.

Cool season precipitation events were associated with air masses originating primarily in inland areas north-northwest of the study area, with a component originating near the Gulf of Mexico. In the absence of seasonal biogenic emissions, these events exhibited overall lower aerosol optical property values and showed evidence of organic emissions from biomass burning. Cool season frontal precipitation was strongly influenced by air masses originating to the northwest of the study area, and also from coastal areas near the Gulf of Mexico and the Atlantic Ocean, while cool season non-frontal events were largely characterized by northwest flow snowfall. While consistent with the presence of smaller, biomass burning particles, aerosol optical properties were not important in determining intensity of precipitation during the cool season.

Values of α_{abs} consistently and significantly increase from beginning to maturation hour, as well as from light to heavy precipitation, during precipitation events in this study. This trend may have been related to a relatively higher fraction of water soluble organic carbon compounds coalescing and serving as effective CCN during the warm season, which ultimately enhanced precipitation. Another possible explanation for this trend may be the aging and/or mixing state of aerosols impacting AppalAIR

ACPD
12, 5487–5517, 2012

during precipitation events in both seasons. Freshly emitted soot particles are more hydrophobic than organic particles. However, if organic particles are emitted locally and soot particles are advected from some distance away, the soot particles may experience atmospheric aging and mixing with sulfate particles. This would result in soot particles that are more hygroscopic and scattering than freshly emitted organics. Therefore, the trend in α_{abs} values may have indicated the raining out of coated or mixed soot particles at maturation or during heavy precipitation, although further research is necessary to provide more conclusive evidence. Generally, AppalAIR is not primarily subject to local pollution sources, but seems to be more strongly impacted by secondary organic aerosols from local biogenic emissions in the warm season.

Acknowledgements. The authors gratefully acknowledge the many NWS COOP and CoCoRaHS precipitation observers, as well as the NOAA Air Resources Laboratory (ARL) for the provision of the HY-SPLIT transport and dispersion model (http://www.arl.noaa.gov/ready.php) used in this publication. NCEP Reanalysis data was provided by the NOAA/Office of Oceanic and Atmospheric Research/Earth System Research Laboratory Physical Sciences Division, Boulder, Colorado, USA, from their Web site at http://www.esrl.noaa.gov/psd/. C. Konrad offered advice in the design of the synoptic classification scheme, and D. Miller, H. Neufeld, and R. Emanuel also offered helpful comments on the research design.

References

Anderson, T. L. and Ogren, J. A.: Determining aerosol radiative properties using the TSI 3563 Integrating Nephelometer, Aerosol Sci. Tech., 29, 57–69, 1998.

Andreae, M. O., Rosenfeld, D, Artaxo, P., Costa, A. A., Frank, G. P., Longo, K. M., and Silva-Dias, M. A. F.: Smoking Rain Clouds over the Amazon, Science, 303, 1337–1342, 2004.

Barr, J. G., Fuentes, J. D., and Bottenheim, J. W.: Radiative forcing of phytogenic aerosols, J. Geophys. Res., 108, 1–13, doi:10.1029/2002JD002978, 2003.

Bell, T. L., Rosenfeld, D., Kim, K. M., Yoo, J. M., Lee, M. I., and Hahnenberger, M.: Midweek increase in U.S. summer rain and storm heights suggests air pollution invigorates rainstorms, J. Geophys. Res., 113, D02209, doi:10.1029/2007JD008623, 2008.

ACPD

12, 5487–5517, 2012

Bergstrom, R. W., Russell, P. B., and Hignett, P.: Wavelength dependence of the absorption of black carbon particles: Predictions and results from the TARFOX Experiment and implications for aerosol single scattering albedo, J. Atmos. Sci., 59, 567–577, 2002.
Bollasina, M., Nigam, S., and Lau, K. M.: Absorbing aerosols and summer Monsoon evolution over South Asia: An observational portrayal, J. Climate, 21, 3221–3239, 2007.
Bond, T. C., Anderson, T. L., and Campbell, D.: Calibration and intercomparison of filter-based measurements of visible light absorption by aerosols, Aerosol Sci. Tech., 30, 582–600, 1999.
Borys, R. D., Lowenthal, D. H., Cohn, S. A., and Brown, W. O. J.: Mountaintop and radar measurements of anthropogenic aerosol effects on snow growth and snowfall rate, Geophys. Res. Lett., 30, 1538, doi:10.1029/2002GL016855, 2003.
Brankov, E., Rao, S. T., and Porter, P. S.: A trajectory-clustering-correlation methodology for examining the long-range transport of air pollutants, Atmos. Environ., 32, 1525–1534, 1998.
Cifelli, R., Doesken, N., Kennedy, P., Carey, L. D., Rutledge, S. A., Gimmestad, C., and Depue, T.: The Community Collaborative Rain, Hail, and Snow Network, B. Am. Meteorol. Soc., 86, 1069–1077, 2005.
Dorling, S. R., Davies, T. D., and Pierce, C. E.: Cluster analysis: a technique for estimating the synoptic meteorological controls on air and precipitation chemistry-Results from Eskdalemuir, South Scotland, Atmos. Environ., 26A, 2583–2602, 1992.
Draxler, R. R.: HYSPLIT4 user's guide, NOAA Tech. Memo, ERL ARL-230, NOAA Air Resources Laboratory, Silver Spring, MD, 1999.
Draxler, R. R. and Rolph, G. D.: HYSPLIT (HYbrid Single-Particle Lagrangian Integrated Trajectory) Model access via NOAA ARL READY Website at http://ready.arl.noaa.gov/HYSPLIT.php, NOAA Air Resources Laboratory, Silver Spring, MD, 2011.
Givati, A. and Rosenfeld, D.: Quantifying Precipitation Suppression Due to Air Pollution, J. Appl. Meteorol., 43, 1038–1056, 2004.
Givati, A. and Rosenfeld, D.: Separation between cloud-seeding and air-pollution effects, J. Appl. Meteorol., 44, 1298–1314, 2005.
Goldstein, A. H., Koven, C. D., Heald, C. L., and Fung, I. Y.: Biogenic carbon and anthropogenic pollutants combine to form a cooling haze over the southeastern United States, P. Natl. Acad. Sci. USA, 106, 8835–8840, 2009.
Holben, B. N., Tanré, D., Smirnov, A., Eck, T. F., Slutsker, I., Abuhassan, N., Newcomb, W. W., Schafer, J. S., Chatenet, B., Lavenu, F., Kaufman, Y. J., Vande Castle, J., Setzer, A., Markham, B., Clark, D., Frouin, R., Halthore, R., Karneli, A., O'Neill, N. T., Pietras, C.,

ACPD
12, 5487–5517, 2012

Pinker, R. T., Voss, K., and Zibordi, G.: An emerging ground-based aerosol climatology: aerosol optical depth from AERONET, J. Geophys. Res., 106, 12067–12097, 2001.
Jirak, I. L. and Cotton, W. R.: Effect of air pollution on precipitation along the Front Range of the Rocky Mountains, J. Appl. Meteorol. Clim., 45, 236–245, 2005.
Kalnay, E., Kanamitsu, M., Kistler, R., Collins, W., Deaven, D., Gandin, L., Iredell, M., Saha, S., White, G., Woollen, J., Zhu, Y., Leetmaa, A., Reynolds, R., Chelliah, M., Ebisuzaki, W., Higgins, W., Janowiak, J., Mo, K. C., Ropelewski, C., Want, J., Jenne, R., and Joseph, D.: The NCEP/NCAR reanalysis 40-year project, B. Am. Meteorol. Soc., 77, 437–471, 1996.
Karl, T.R., Melillo, J. M., and Peterson, T. C.: Global Climate Change Impacts in the United States, Cambridge University Press, New York, NY, 2009.
Keighton, S., Lee, L., Holloway, B., Hotz, D., Zubrick, S., Hovis, J., Votaw, G., Perry, L. B., Lackmann, G., Yuter, S., Konrad, C. E., Miller, D., and Etherton, B.: A collaborative approach to better understanding northwest flow snowfall in the southern Appalachians, B. Am. Meteorol. Soc., 90, 979–991, 2009.
Keim, B. D.: Spatial, synoptic, and seasonal patterns of heavy rainfall in the southeastern United States, Phys. Geogr., 17, 313–328, 1996.
Kelly, G. M., Perry, L. B., Taubman, B. F., and Soulé, P. T.: Synoptic classification of precipitation events in the southern Appalachian Mountains, Clim. Res., under review, 2012.
Khain, A., Pokrovsky, A., and Pinsky, M.: Simulation of Effects of Atmospheric Aerosols on Deep Turbulent Convective Clouds Using a Spectral Microphysics Mixed-Phase Cumulus Cloud Model. Part I: Model Description and Possible Applications, J. Atmos. Sci., 61, 2963–2982, 2004.
Konrad, C. E.: Synoptic-scale features associated with warm season heavy rainfall over the interior southeastern United States, Weather Forecast., 12, 557–571, 1997.
Li, W., Li, L., Fu, R., Deng, Y., and Wang, H.: Changes to the North Atlantic Subtropical High and its role in the intensification of summer rainfall variability in the southeastern United States, J. Climate, 24, 1499–1506, 2010.
Lohmann, U. and Hoose, C.: Sensitivity studies of different aerosol indirect effects in mixed-phase clouds, Atmos. Chem. Phys., 9, 8917–8934, doi:10.5194/acp-9-8917-2009, 2009.
Lynn, B. H., Healy, R., and Druyan, L. M.: An Analysis of the Potential for Extreme Temperature Change Based on Observations and Model Simulations, J. Climatol., 20, 1539–1554, 2007.
National Climatic Data Center Service Records Retention System Analysis and Forecast Charts, available at: http://nomads.ncdc.noaa.gov/ncep/NCEP (last access: January 2011),

ACPD
12, 5487–5517, 2012

2010.
National Centers for Environmental Prediction Daily Weather Maps, available at: http://www.hpc.ncep.noaa.gov/dailywxmap/index.html (last access: January 2011), 2010.
National Oceanic and Atmospheric Administration Earth System Research Laboratory Daily Mean Composites, available at: http://www.esrl.noaa.gov/psd/data/composites/day/ (last access: January 2011), 2010.
Perry, L. B., Konrad, C. D., and Schmidlin, T. W.: Antecedent Upstream Air Trajectories Associated with Northwest Flow Snowfall in the Southern Appalachians, Weather Forecast., 22, 334–352, 2007.
Perry, L. B., Konrad, C. E., Hotz, D. G., and Lee, L. G.: Synoptic Classification of Snowfall Events in the Great Smoky Mountains, USA, Phys. Geogr., 31, 156–171, 2010.
Power, H. C., Sheridan, S. C., and Senkbeil, J. C.: Synoptic climatological influences on the spatial and temporal variability of aerosols over North America, Int. J. Climatol., 26, 732–741, 2006.
Prados, A. I., Dickerson, R. R., Doddridge, B. G., Milne, P. A., Moody, J. L., and Merrill, J. T.: Transport of ozone and pollutants from North America to the North Atlantic Ocean during the 1996 Atmosphere/Ocean Chemistry Experiment (AEROCE) intensive, J. Geophys. Res., 104, 26219–26233, doi:10.1029/1999JD900444, 1999.
Rosenfeld, D.: TRMM observed first direct evidence of smoke from forest fires inhibiting rainfall, Geophys. Res. Lett., 26, 3105–3108, 1999.
Rosenfeld, D.: Suppression of rain and snow by urban and industrial air pollution, Science, 287, 1793, doi:10.1126/science.287.5459.1793, 2000.
Rosenfeld, D. and Givati, A.: Evidence of orographic precipitation suppression by air pollution induced aerosols in the western United States, J. Appl. Meteorol. Clim., 45, 893–911, 2006.
Rosenfeld, D., Lahav, R., Khain, A., and Pinsky, M.: The role of sea spray in cleansing air pollution over ocean via cloud processes, Science, 297, 1667–1670, 2002.
Rudich, Y. and Khersonsky, O.: Treating clouds with a grain of salt, Geophys. Res. Lett., 29, 2060, doi:10.1029/2002GL016055, 2002.
Sheridan, P. J., Delene, D. J., and Ogren, J. A.: Four years of continuous surface aerosol measurements from the DOE/ARM Southern Great Plains CART site, Eleventh ARM Science Team Meeting Proceedings, Atlanta, Georgia, 19–23 March, 2001.
Swap, R. M., Garstang, M., Greco, S., Talbot, R., and Kållberg, P.: Saharan dust in the Amazon Basin, Tellus, 44B, 133–149, 1992.

ACPD
12, 5487–5517, 2012

Taubman, B. F., Hains, J. C., Thompson, A. M., Marufu, L. T., Doddridge, B. G., Stehr, J. W., Piety, C. A., and Dickerson, R. R.: Aircraft vertical profiles of trace gas and aerosol pollution over the mid-Atlantic Unites States: Statistics and meteorological cluster analysis, J. Geophys. Res., 111, D10S07, doi:10.1029/2005JD006196, 2006.

U.S. Census Bureau, 2006–2010 American Community Survey, available at: http://www.census.gov/acs/www/ (last access: January 2012), 2010.

Weber, R. J., ASullivan, A. P., Peltier, R. E., Russell, A., Yan, B., Zheng, M., Gouw, J., Warneke, C., Brock, C., Holloway, J. S., Atlas, E. L., and Edgerson, E.: A study of secondary organic aerosol formation in the anthropogenic-influenced southeastern United States, J. Geophys. Res., 112, D13302, doi:10.1029/2007JD008408, 2007.

ACPD
12, 5487–5517, 2012

Table 1. Instruments and aerosol measurements made at AppalAIR. Absorption Ångström exponent value calculated using based on Delene and Ogren (2002).

Instrument	Primary measurement	Derived measurements	Description of Intensive Property
TSI Model 3563 three-wavelength (450, 550, and 700 nm) integrating nephelometer	Total scattering and hemispheric backscattering coefficients (σ_{sp} *and* σ_{bsp}) at 450, 550, 700 nm, for particles with aerodynamic diameters less than 10μm and less than 1 μm	Hemispheric backscatter fraction, $b = \sigma_{bsp}/\sigma_{sp}$	b provides a qualitative indicator of particle size, with higher (lower) values corresponding to smaller (larger) particles.
		Single scattering albedo at 550 nm, $\omega_o = \sigma_{sp}/(\sigma_{sp} + \sigma_{ap})$	ω_o provides an indicator of the relative contributions of absorption and scattering to total light extinction.
		Scattering Ångström exponent, $\alpha_{scat} = -\log[\sigma_{sp}(450)/\sigma_{sp}(700)]/\log[450/700]$	α_{scat} is a measure of the spectral dependence of aerosol light scattering, providing a means for broadly classifying aerosol size.
Radiance Research three-wavelength (467, 530, 660 nm) Particle Soot Absorption Photometer (PSAP)	Light absorption coefficient (σ_{abs}) at 467, 530, and 660 nm, for particles with aerodynamic diameters less than 10 μm and less than 1 μm	Absorption Ångström exponent, $\alpha_{abs} = -\log[\sigma_{abs}(467)/\sigma_{abs}(660)]/\log[467/660]$ (Delene and Ogren, 2002)	α_{abs} is a measure of the spectral dependence of aerosol light absorption, providing a means for broadly classifying aerosol types.

ACPD
12, 5487–5517, 2012

Table 2. Seasonal summaries of precipitation events. Average total precipitation values from COOP and CoCoRaHS stations in study area. Average temperature, relative humidity, wind speed, and wind direction are from the BEECHTOP meteorological station.

Season	*n*	Average Spatial Coverage (%)	Avg. Total Precip (mm)	Temperature (°C)	Relative Humidity (%)	Wind Speed ($m\,s^{-1}$)	Wind Direction (degrees)	Most Frequent Wind Direction(s) (degrees)
Warm	123	80	8.9	15.8	95.6	3.4	244 (SW)	S, NW
Cool	60	69	13.4	−1.6	98.0	5.0	172 (S)	SSE, NW

ACPD
12, 5487–5517, 2012

Table 3. Differences in mean meteorological and aerosol values at beginning-6 h and maturation for all warm season events versus all cool season precipitation events, plus difference in values from beginning-6 h. to maturation. P-values (2-tailed) italicized in bold indicate significance at the 95 % confidence interval or greater. An asterisk (*) indicates values obtained using a parametric test.

	All Warm	All Cool	Abs Diff	p-value						
	$n = 123$	$n = 60$								
Avg. Precip (mm)	8.9	13.6	4.7	0.945						
	Beginning-6 h				Maturation				Diff. from Beg-6-Mat	
	All Warm	All Cool	Abs Diff	p-value	All Warm	All Cool	Abs Diff	p-value	All Warm	All Cool
Meteorological Values									p-value	p-value
Beech T (°C)	61.3	30.1	31.2	***0.000****	15.3	−2.2	17.49	***.000****	***−0.006****	−0.416*
Beech RH (%)	92.4	90.2	2.2	0.721	96.2	98.8	2.6	0.205	***+0.000***	***+0.000***
Beech WS ($m\,s^{-1}$)	7.5	10.7	3.2	***0.001***	3.7	5.7	2.1	***0.004***	+0.107	+0.487
Beech WD (degrees)	232 (SW)	195 (SSW)	37	NA	244 (WSW)	176 (S)	68	NA	NA	NA
Aerosol Values										
Scattering	57.43	28.24	29.19	***0.000***	45.08	16.58	28.5	***0.000***	***−0.002***	***−0.001***
Absorption	3.49	3.71	0.22	0.566	3.20	2.40	0.80	***0.002***	***−0.003***	***−0.001***
b	0.12	0.15	0.03	***0.000***	0.13	0.16	0.04	***0.000***	+0.237	+0.101
ω_o	0.93	0.87	0.06	***0.000***	0.92	0.84	0.07	***0.000***	−0.329	−0.222
a_{scat}	1.97	2.07	0.10	***0.003***	1.95	2.16	0.21	***0.000***	−0.565	***+0.003***
a_{abs}	0.42	0.95	0.53	***0.000****	0.58	1.20	0.62	***.000****	***+0.000****	***+0.000****

ACPD
12, 5487–5517, 2012

Table 4. Differences in mean meteorological and aerosol values at beginning-6 h. and maturation between light versus heavy warm season precipitation events, plus difference in values from beginning-6 h. to maturation. *P*-values (2-tailed) italicized in bold indicate significance at the 95 % confidence interval or greater. An asterisk (*) indicates values obtained using a parametric test.

	Light	Heavy	Abs Diff	p -value						
	n = 31	*n* = 31								
Avg. Precip (mm)	2.1	20	17.9	*0.000**						
	Beginning-6 h				Maturation				Diff. from Beg-6-Mat	
	Light	Heavy	Abs Diff	p-value	Light	Heavy	Abs Diff	p-value	Light	Heavy
Meteorological Values									p-value	p-value
Beech *T* (°C)	14.4	15.4	1.0	***0.012****	14.4	15.4	1.0	0.187*	−0.423*	−0.084*
Beech RH (%)	96.0	95.7	0.3	0.224	96	95.7	0.3	0.844	***+0.012***	***+0.002***
Beech WS ($m\,s^{-1}$)	4.1	3.8	0.3	***0.007****	4.1	3.8	0.3	0.563*	+0.997*	+0.060
Beech WD (degrees)	232 (SW)	215 (SW)	17	NA	254 (WSW)	184 (S)	70	NA	NA	NA
Aerosol Values										
Scattering	56.43	59.09	2.66	0.863	51.17	34.59	16.58	***0.012***	−0.483*	***−0.016***
Absorption	3.45	3.35	0.10	0.791*	3.51	2.83	0.68	0.149	+0.917*	***−0.035***
b	0.13	0.12	0.01	0.388*	0.13	0.13	0.00	0.835	−0.829	+0.200
ω_o	0.93	0.91	0.02	0.669	0.93	0.88	0.05	0.276	−0.676*	−0.437
a_{scat}	2.04	1.96	0.08	0.147*	2.05	1.92	0.13	***0.022****	+0.718	−0.341*
a_{abs}	0.40	0.41	0.01	0.917*	0.48	0.70	0.22	***0.016****	+0.265*	***+0.004****

ACPD
12, 5487–5517, 2012

Table 5. Differences in mean meteorological and aerosol values at beginning-6 h. and maturation between light versus heavy cool season precipitation events, plus difference in values from beginning-6 h. to maturation. P-values (2-tailed) italicized in bold indicate significance at the 95 % confidence interval or greater. An asterisk (*) indicates values obtained using a parametric test.

	Light	Heavy	Abs Diff	p-value						
	$n = 15$	$n = 15$								
Avg. Precip (mm)	1.3	39.3		*0.000**						
	Beginning-6 h				Maturation				Diff. from Beg-6-Mat	
	Light	Heavy	Abs Diff	p-value	Light	Heavy	Abs Diff	p-value	Light	Heavy
Meteorological Values									p-value	p-value
Beech *T* (°C)	−4.5	3.1	7.6	***0.001***	−4.8	2.6	7.44	***0.001****	+0.974*	−0.802*
Beech RH (%) 96.9	80.5	16.4	***0.002***	99.1	99.9	0.88	0.062	+0.325	***+0.000***	
Beech WS ($m\,s^{-1}$)	3.5	7.2	3.7	***0.004***	3.4	9.5	6.1	***0.001****	−0.612	+0.177*
Beech WD (degrees)	286 (W)	163 (SSE)	123	NA	256 (WSW)	142 (SE)	114	NA	NA	NA
Aerosol Values										
Scattering	16.09	42.42	26.33	***0.058***	14.28	15.95	1.67	0.835	−0.724	***+0.000***
Absorption	1.82	5.90	4.08	***0.000****	2.75	2.36	0.39	0.297	+0.983	***+0.000***
b	0.15	0.14	0.01	0.193*	0.17	0.16	0.01	0.531	+0.576	+0.099*
ω_o	0.87	0.86	0.01	***0.021***	0.82	0.83	0.01	0.531	−0.950	***−0.008***
a_{scat}	2.08	1.98	0.10	0.121*	2.19	1.97	0.22	0.192*	+0.215*	−0.959*
a_{abs}	0.91	0.99	0.08	0.132*	1.24	1.28	0.04	0.669*	***+0.000****	***+0.001****

ACPD
12, 5487–5517, 2012

Table 6. Differences in mean meteorological and aerosol values at beginning-6 h and maturation between warm season frontal and non-frontal precipitation events, plus difference in values from beginning-6 h. to maturation. P-values (2-tailed) italicized in bold indicate significance at the 95 % confidence interval or greater. An asterisk (*) indicates values obtained using a parametric test.

	Warm Frontal	Warm Non-Frontal	Abs Diff	p-value						
	$n = 60$	$n = 63$								
Avg. Precip (mm)	10.2	7.6	2.6	0.231						
	Beginning-6 h				Maturation				Diff. from Beg-6-Mat	
	Warm Frontal	Warm Non-Frontal	Abs Diff	p-value	Warm Frontal	Warm Non-Frontal	Abs Diff	p-value	Warm Frontal	Warm Non-Frontal
Meteorological Values									p-value	p-value
Beech T (°C)	61	61.5	0.5	0.575*	14.9	15.7	0.8	0.110*	***−0.013****	−0.139*
Beech RH (%)	93.3	91.6	1.7	0.312	97.6	94.9	2.7	0.071	***+0.000***	***+0.000***
Beech WS ($m\,s^{-1}$)	7.8	7.3	0.5	0.445	3.8	3.5	0.4	0.256*	−0.177	−0.336
Beech WD (degrees)	248 (WSW)	213 (SSW)	35	NA	271 (W)	207 (SSW)	64	NA	NA	NA
Aerosol Values										
Scattering	53.38	61.23	7.85	0.137	39.40	50.11	10.71	0.072	***−0.012***	−0.066*
Absorption	3.20	3.75	0.55	0.094	3.20	3.19	0.01	0.255	+0.050	***−0.017***
b	0.12	0.12	0.00	0.065	0.13	0.12	0.01	0.165	+0.582	+0.293
ω_o	0.93	0.93	0.00	0.945	0.92	0.92	0.00	0.352	−0.224	−0.897
a_{scat}	1.99	1.95	0.04	0.285	1.97	1.92	0.05	0.284*	−0.771	−0.513*
a_{abs}	0.44	0.41	0.03	0.610*	0.60	0.57	0.04	0.563*	***+0.010****	***+0.006****

ACPD
12, 5487–5517, 2012

Table 7. Mean precipitation (mm) values associated with lower and upper quartile aerosol values during warm season frontal and non-frontal precipitation events.

	Frontal Precipitation Events							
	Beginning-6 h				Maturation			
	Lower ($n = 15$)	Upper ($n = 15$)			Lower ($n = 15$)	Upper ($n = 15$)		
Aerosol Values	Precip	Precip	Abs Diff	p-value	Precip	Precip	Abs Diff	p-value
Scattering	10.0	12.0	2.0	0.777	7.6	13.0	5.4	0.232
Absorption	11.6	6.6	5	0.394	8.3	11.8	3.5	0.801
b	6.9	10.2	3.3	0.192	10.6	9.2	1.4	0.783
ω_o	9.1	10.3	1.2	0.301	9.0	11.8	2.8	0.804
a_{scat}	5.1	9.8	4.7	0.077	9.3	10.1	0.8	0.646
a_{abs}	8.3	8.2	0.1	0.957	10.5	10.5	0.0	0.762
	Non-frontal Precipitation Events							
	Beginning-6 h				Maturation			
	Lower ($n = 16$)	Upper ($n = 16$)			Lower ($n = 16$)	Upper ($n = 16$)		
Aerosol Value	Precip	Precip	Abs Diff	p-value	Precip	Precip	Abs Diff	p-value
Scattering	6.5	7.3	0.8	0.678	1.2	5.5	4.3	***0.017***
Absorption	8.8	7.6	1.2	0.527	8.2	5.2	3.0	0.224
b	14.9	17.0	2.1	0.533*	6.2	7.7	1.5	0.838
ω_o	7.5	4.6	2.9	0.060	1	5.8	4.8	0.160
a_{scat}	7.5	4.6	2.9	0.136*	8.7	3.7	5.0	***0.001***
a_{abs}	6.5	9.9	3.4	0.073	6.1	12.6	6.5	***0.010***

ACPD
12, 5487–5517, 2012

Table 8. Differences in mean meteorological and aerosol values at beginning-6 h and maturation between light and heavy warm season non-frontal precipitation events, plus difference in values from beginning-6 h. to maturation. P-values (2-tailed) italicized in bold indicate significance at the 95 % confidence interval or greater. An asterisk (*) indicates values obtained using a parametric test.

	Warm Non-frontal Light $n = 16$	Warm Non-frontal Heavy $n = 16$	Abs Diff	p-value						
Avg. Precip (mm)	2.1	16.4	14.3	*0.000*						
	Beginning-6 h				Maturation				Diff. from Beg-6 h To Mat	
	Warm Non-frontal Light	Warm Non-frontal Heavy	Abs Diff	p-value	Warm Non-frontal Light	Warm Non-frontal Heavy	Abs Diff	p-value	Warm Non-frontal Light	Warm Non-frontal Heavy
Meteorological Values									p-value	p-value
Beech T (°C)	15.6	16.1	0.5	0.617*	15.4	15.3	0.1	0.921*	0.972*	−0.612*
Beech RH (%)	91.8	94.0	2.2	0.817	93.1	96.9	3.8	0.601	−0.982	0.153
Beech WS ($m\,s^{-1}$)	3.8	3.4	0.4	0.228	3.7	4.1	0.4	0.499*	+0.945*	+0.551*
Beech WD (degrees)	184 (S)	195 (SSW)	11	NA	182 (S)	170 (S)	12	NA	NA	NA
Aerosol Values										
Scattering	65.77	54.42	11.35	0.373*	58.67	30.43	28.24	***0.006****	−0.970	−0.199*
Absorption	3.93	3.56	0.37	0.309	3.46	2.33	1.13	0.082	−0.850	−0.206*
b	0.12	0.12	0.00	0.553	0.12	0.13	0.01	0.347*	0.850	+0.206*
ω_o	0.94	0.89	0.05	0.167	0.94	0.85	0.09	0.058	0.815*	−0.418
a_{scat}	2.07	1.91	0.16	***0.041****	2.11	1.87	0.24	***0.001****	+0.984*	−0.612*
$-a_{abs}$	0.33	0.48	0.15	0.099*	0.35	0.79	0.44	***0.001****	+0.495*	***+0.020****

ACPD
12, 5487–5517, 2012

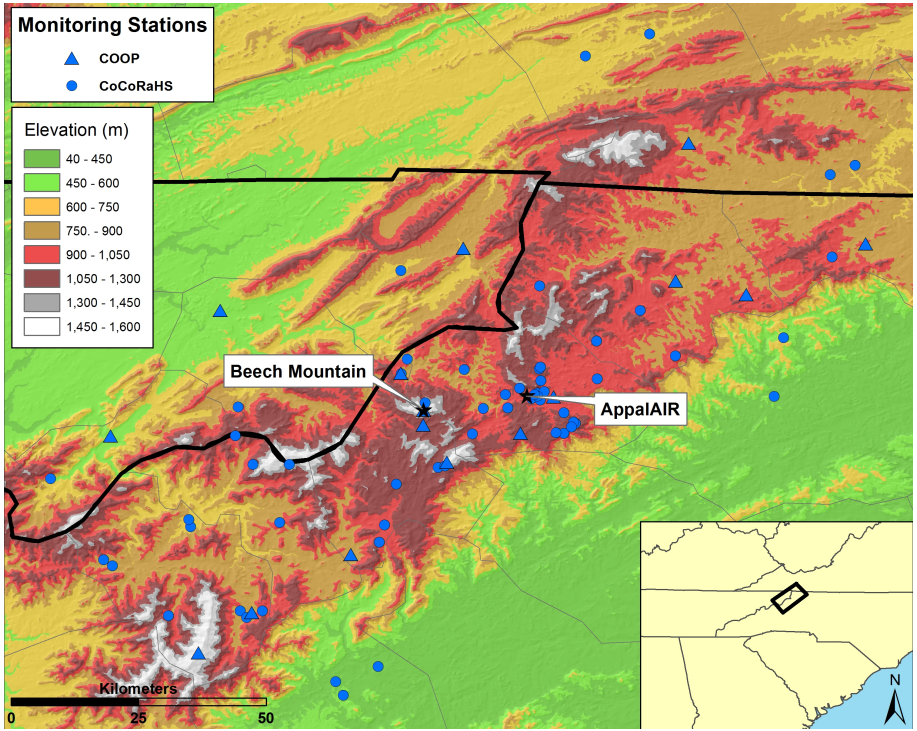

Fig. 1. Topography of study area, including locations of AppalAIR, Beech Mountain, and COOP and CoCoRaHS stations.

ACPD
12, 5487–5517, 2012

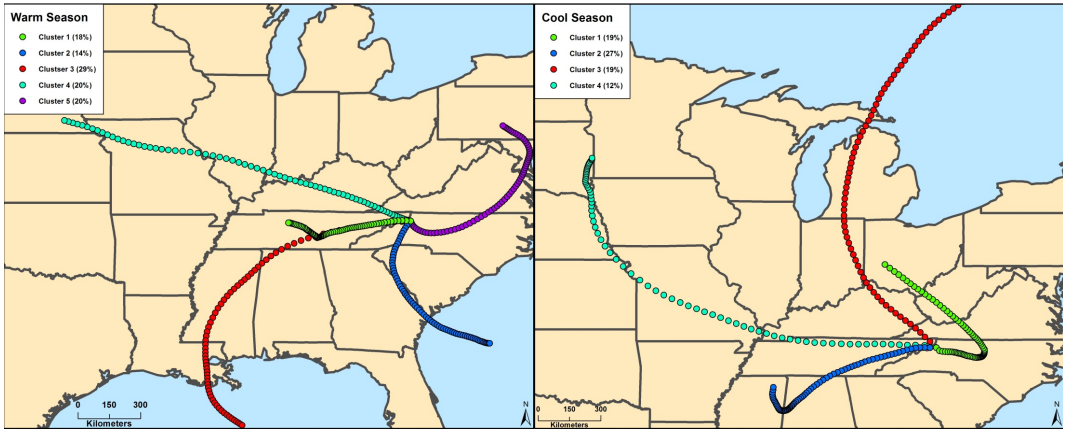

Fig. 2. HYSPLIT cluster analysis of backward air trajectories representing maturation hour of each precipitation event during warm season (left) and cool season (right). Colored lines represent the mean trajectory of each cluster. Clusters are numbered and values in parentheses represent the percentage of backward air trajectories included in each cluster. Trajectories terminating before 72 h, likely as a result of missing meteorological data, were NOT included in the clustering.

ACPD
12, 5487–5517, 2012

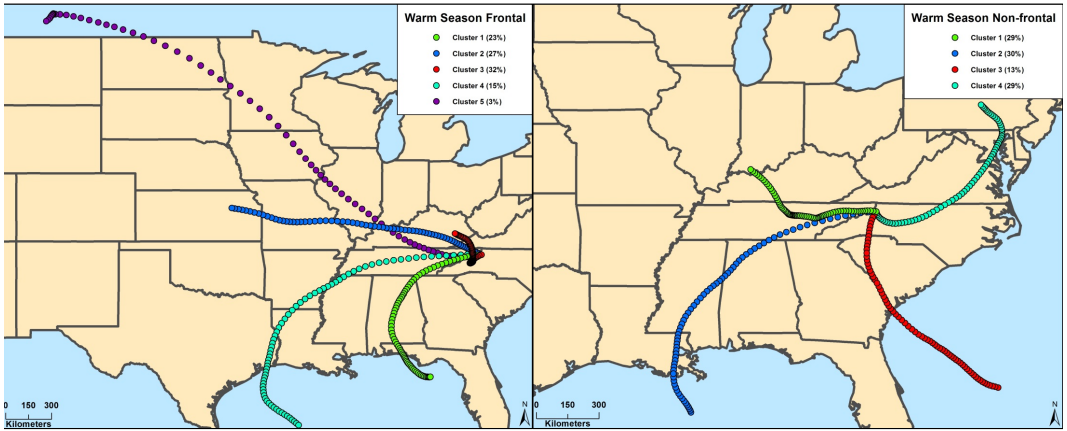

Fig. 3. HYSPLIT cluster analysis of backward air trajectories representing maturation hour of warm season frontal (left) and non-frontal (right) precipitation events. Colored lines represent the mean trajectory of each cluster. Clusters are numbered and values in parentheses represent the percentage of backward air trajectories included in each cluster.

ACPD
12, 5487–5517, 2012